Theory of waves in pair-ion plasmas: Natural explanation of backward modes

M. Kono, J. Vranjes, and N. Batool

Citation: Physics of Plasmas **20**, 122111 (2013); doi: 10.1063/1.4846895
View online: http://dx.doi.org/10.1063/1.4846895
View Table of Contents: http://scitation.aip.org/content/aip/journal/pop/20/12?ver=pdfcov
Published by the AIP Publishing

Theory of waves in pair-ion plasmas: Natural explanation of backward modes

M. Kono,[1] J. Vranjes,[2] and N. Batool[3]
[1]*Faculty of Policy Studies, Chuo University, Tokyo, Japan*
[2]*Institute of Physics, Belgrade, Serbia*
[3]*National Center for Physics, Islamabad, Pakistan*

(Received 8 November 2013; accepted 29 November 2013; published online 13 December 2013)

Backward waves observed in the experiments by Oohara and Hatakeyama (Phys. Rev. Lett. **91**, 205005 (2003)) are identified to be ion cyclotron harmonic waves inherent to the kinetic theory. The derived dispersion equation is based on exact solutions of the characteristic equations of the Vlasov equation in a bounded cylindrical coordinate system; it is different from its counterpart in unbounded plasmas, and it provides all the branches of the dispersion relations observed in the experiment. Positive and negative ions respond to a potential in the same time scale and cooperate to expose kinetic orbital behaviors to the macroscopic propagation characteristics. In addition, the experimental setting of the large Larmor radius makes higher harmonic ion cyclotron backward/forward waves observable. The large Larmor radius effects are naturally treated by a kinetic theory. © *2013 AIP Publishing LLC*. [http://dx.doi.org/10.1063/1.4846895]

I. INTRODUCTION

After the pioneering experimental studies on propagation properties of electrostatic waves in pair-ion plasmas,[1–5] there have appeared a number of theoretical works on various linear and nonlinear modes in pair-ion plasmas.[6–17] However, quite a number of basic propagation characteristics observed in the experiments have not been explained yet. In the experiments, at least three kinds of electrostatic waves propagating parallel to the external magnetic field are reported. These are classified according to high ($\omega > \sqrt{2}\omega_p$), intermediate ($\Omega < \omega < \sqrt{2}\omega_p$), and low ($\omega < \Omega$) frequency waves, where ω_p and Ω are the ion plasma frequency and the ion cyclotron frequency, respectively. It is reported that the high and low frequency waves are, respectively, the familiar ion plasma wave and the ion sound wave. The intermediate frequency wave has not been identified yet. This is a backward mode for which the sign of the group velocity is opposite to that of the phase velocity.

The above classification regarding the frequency range is based on theories of unbounded plasmas and this has been the origin of various confusions that could be summarized as follows. (1) In a cylindrical system, the dispersion relation of the ion Langmuir wave in a pair-ion plasma is not $2^{1/2}\omega_p$; in fact, it is $[2k_z^2/(k_\perp^2 + k_z^2)]^{1/2}\omega_p$. (2) Since ion cyclotron waves survive only for $k_\perp \gg k_z$ due to the Landau damping, longitudinal intermediate frequency waves cannot be excited. (3) In usual plasmas, ion sound waves are excited only when electrons coexist. In view of this and the fact that sound-type waves are observed in the experiments,[1–5] some authors have claimed that the plasma produced in the experiment is not really a pure pair-ion plasma but a plasma with electrons. (4) Although the observed potential is clearly spatially peaked at the center of the vessel, the backward wave is claimed by some authors to be a surface wave, which may be related to (2). (5) Finally, there exists a problem of terminology as well. In pure pair-ion plasmas, the ion sound wave is termed as "ion thermal wave" or "ordinary sound wave" in order to stress explicitly that electrons do not exist.

In spite of negative discussions on the observed dispersion relations, the more than three dispersion curves including a tiny fragments (which has also remained unexplained so far) are lined up in the (k_z, ω) plane, and each dispersion curve is settled within the width of 2Ω, suggesting that the kinetic cyclotron harmonic resonances play a crucial role. A main feature of pair-ion plasmas is that positive and negative ions respond to a potential in the same time scale and expose the kinetic orbital behaviors to the level of the macroscopic properties like propagation characteristics.

Due to these reasons, in this paper, we develop a kinetic theory in a cylindrical coordinate system to treat all eigenmodes in a unified manner. Since the experiments are done in a thin cylindric vessel, the kinetic theory is formulated in a suitable cylindrical coordinate system. Exact solutions of the characteristic equations of the linearized Vlasov equation are obtained and the dielectric function is derived after integrating the linearized Vlasov equation along the orbit. The even and odd cyclotron resonances are separated in the direction parallel and perpendicular to the magnetic field in contrast to those in unbounded plasmas. The backward waves are identified to be ion cyclotron harmonic waves. The large Larmor radius under the experimental conditions brings higher harmonic cyclotron resonances to participate in the dispersion equations, resulting in the first few harmonic ion cyclotron forward/backward waves observable.

The dispersion curves of the analytically obtained low and high frequency backward waves are terminated at certain wavenumber k_z and this happens not due to the cyclotron damping but due to the fact that solutions of dispersion equations become complex. In a cylindrical system, the orbit in phase space is rather complicated due to the centrifugal force and the cyclotron resonance damping is not effective since particles are unlikely to come back to the same phase of the wave after one cyclotron period.

In Sec. II, we derive exact solutions for the characteristic equations of the linearized Vlasov equation and integrate the Vlasov equation in time along the exact orbit to derive the current. In Sec. III, we derive the dispersion equation given by the boundary condition together with the subsidiary condition, which determines the perpendicular wavenumber. In Sec. IV, we solve the dispersion equation to obtain two backward waves in low and intermediate frequency ranges. These backward waves are identified to be ion cyclotron harmonic waves. In the low frequency range, the ion cyclotron backward wave is coupled with the ion thermal mode which is a forward wave, and both modes are terminated at a finite wavenumber. In Sec. V, we discuss forward waves, that is, the ion cyclotron wave and the ion Langmuir wave. Summary and discussion are given in Sec. VI.

II. DERIVATIONS OF DIELECTRIC FUNCTIONS

For a plasma confined in a cylindrical vessel immersed in a constant magnetic field **B** in the axial z direction, we solve the Vlasov equation for electrostatic perturbations in cylindrical coordinates

$$\frac{\partial}{\partial t}F_\alpha+\left(v_r\frac{\partial}{\partial r}+\frac{v_\theta}{r}\frac{\partial}{\partial\theta}+v_z\frac{\partial}{\partial z}\right)F_\alpha + \left[\left(\Omega_\alpha v_\theta+\frac{v_\theta^2}{r}\right)\frac{\partial}{\partial v_r}-\left(\Omega_\alpha v_r+\frac{v_r v_\theta}{r}\right)\frac{\partial}{\partial v_\theta}\right]F_\alpha = \frac{e_\alpha}{m_\alpha}\left(\frac{\partial\phi}{\partial r}\frac{\partial}{\partial v_r}+\frac{1}{r}\frac{\partial\phi}{\partial\theta}\frac{\partial}{\partial v_\theta}+\frac{\partial\phi}{\partial z}\frac{\partial}{\partial v_z}\right)F_\alpha, \tag{1}$$

where $\Omega_\alpha=e_\alpha B/m_\alpha c$ and α denote the species as $\alpha=\pm$, and we obtain the dielectric functions from the equation

$$\nabla\cdot\left[\frac{\partial\mathbf{E}(\mathbf{r},t)}{\partial t}+\sum_\alpha 4\pi n_{0\alpha}e_\alpha\int\mathbf{v}F_\alpha(\mathbf{r},\mathbf{v},t)d\mathbf{v}\right]=0, \tag{2}$$

which is derived from the continuity and the Poisson equations. The equilibrium is given by $F_{\alpha0}(\mathbf{v})=F_{\alpha0}(v_\perp,v_z)$, where $v_\perp^2=v_r^2+v_\theta^2$, and we choose $F_{\alpha0}$ to be Maxwellian. Now, we introduce a fluctuation f_α through

$$F_\alpha(\mathbf{r},\mathbf{v},t)=F_{\alpha0}(v_\perp,v_z)+f_\alpha(\mathbf{r},\mathbf{v},t), \tag{3}$$

and linearize Eq. (1) to get

$$\frac{df_\alpha}{dt}=\frac{e_\alpha}{m_\alpha}\left(\frac{\partial\phi}{\partial r}\frac{\partial}{\partial v_r}+\frac{1}{r}\frac{\partial\phi}{\partial\theta}\frac{\partial}{\partial v_\theta}+\frac{\partial\phi}{\partial z}\frac{\partial}{\partial v_z}\right)F_{\alpha0}, \tag{4}$$

where d/dt is the total derivative. Equation (4) is integrated along the characteristic orbit in the phase space, which is defined by

$$\frac{dr}{dt}=v_r,\quad \frac{d\theta}{dt}=\frac{v_\theta}{r},\quad \frac{dz}{dt}=v_z,\quad \frac{dv_z}{dt}=0,$$
$$\frac{dv_r}{dt}=\frac{v_\theta^2}{r}+\Omega_\alpha v_\theta,\quad \frac{dv_\theta}{dt}=-\frac{v_\theta v_r}{r}-\Omega_\alpha v_r. \tag{5}$$

Since we have three invariants, kinetic energy $E=v_r^2+v_\theta^2=v_\perp^2$, canonical angular momentum $L=v_\theta r+(\Omega_\alpha/2)r^2$, and velocity parallel to the magnetic field v_z, we may introduce a variable $\varphi(t)$ through $v_r=v_\perp\cos\varphi$ and $v_\theta=v_\perp\sin\varphi$. Equations for $\varphi(t)$ and $\theta(t)$ then reduce to

$$\frac{d\varphi}{dt}=-\frac{v_\perp}{r}\sin\varphi-\Omega_\alpha,\quad \frac{d\theta}{dt}=-\frac{d\varphi}{dt}-\Omega_\alpha, \tag{6}$$

where $r(t)=r_L[-\varepsilon\sin\varphi(t)+(\sin^2\varphi(t)+2\kappa)^{1/2}]$ is derived from the invariant $L(\kappa=L\Omega_\alpha/v_\perp^2)$, and r_L is the Larmor radius defined by $r_L=v_\perp/|\Omega_\alpha|$ and $\varepsilon=|\Omega_\alpha|/\Omega_\alpha$. Since $r(t)$ is non-negative, $\kappa\geq0$. The two quantities $\varphi(t)$ and $\theta(t)$ are obtained as

$$\varphi(t)=\tilde\varphi_0-\Omega_\alpha t-\varepsilon\sin^{-1}[\cos\varphi(t)/s(\kappa)] =\Phi(t)-\sin^{-1}\frac{\cos\Phi(t)}{\sqrt{2[1+\kappa+\varepsilon s(\kappa)\sin\Phi(t)]}}, \tag{7}$$

$$\theta(t)=\tilde\theta_0+\varepsilon\sin^{-1}[\cos\varphi(t)/s(\kappa)], \tag{8}$$

where $\Phi(t)=\tilde\varphi_0-\Omega_\alpha t$, $s(\kappa)=(1+2\kappa)^{1/2}$, $\tilde\varphi_0=\varphi_0+\sin^{-1}[\cos(\varphi_0/s(\kappa))]$, $\varphi_0=\varphi(0)$, $\tilde\theta_0=\theta_0-(\tilde\varphi_0-\varphi_0)$, and $\theta_0=\theta(0)$. The $r(t)$ and $z(t)$ are integrated as

$$r(t)=r_L\sqrt{2[1+\kappa+\varepsilon s(\kappa)\sin\Phi(t)]}+\tilde r_0 =r_L p(\kappa)\sin\psi(t)+\tilde r_0, \tag{9}$$

$$z(t)=v_z t+z_0, \tag{10}$$

where

$$\psi(t)=\cos^{-1}[q(\kappa)\cos(\Phi(t)/2+\varepsilon\pi/4)],$$
$$p(\kappa)=\sqrt{2[1+\kappa+s(\kappa)]},\quad q(\kappa)=2s(\kappa)/p(\kappa),$$
$$\tilde r_0=r_0-r_L\sqrt{1+\kappa+\varepsilon s(\kappa)\sin\tilde\varphi_0},\ r_0=r(0),\ \text{and}\ z_0=z(0).$$

Since the exact solutions Eqs. (8) and (9) are not simply applicable to time integration of Eq. (4) along the orbit, we use the following approximation. Noting $s(\kappa)\geq1$ and $|\cos\varphi/s(k)|\leq1$, $\theta(t)$ is approximated as

$$\theta(t)\simeq\tilde\theta_0+\varepsilon S(\kappa)\cos\Phi(t),\quad S(\kappa)=\sin^{-1}[1/s(\kappa)]. \tag{11}$$

In a similar way using the conditions $q(\kappa)\leq1$ and $|q(\kappa)\cos\psi(t)|\leq1$ in Eq. (9), we may approximate $\psi(t)$ as

$$\psi(t)\simeq\pi/2+Q(\kappa)\cos[\Phi(t)/2+\varepsilon\pi/4],\quad Q(\kappa)=\sin^{-1}q(\kappa), \tag{12}$$

leading to

$$r(t)=r_L p(\kappa)\sin\psi(t)\simeq r_L p(\kappa)\cos\{Q(\kappa)\cos[\Phi(t)/2+\varepsilon\pi/4]\}, =r_L p(\kappa)\left\{J_0[Q(\kappa)]+2\sum_{n\geq1}J_{2n}[Q(\kappa)]\cos[n(\Phi(t)+\varepsilon\pi/2)]\right\}. \tag{13}$$

Here, J_ℓ is the Bessel function of the first kind and it is a positive definite since $Q(\kappa)$ is smaller than the first zero of J_0. In the following, we retain only J_0 and J_2 since J_{2n} with $n > 2$ is negligible compared with J_0 and J_2.

Now, (r', θ') at t' are represented by (r, θ) at t as

$$r' = r + 2r_L p(\kappa) J_2[Q(\kappa)][\sin(\Omega_\alpha \tau + \varphi) - \sin\varphi], \tag{14}$$

$$\theta' = \theta + \xi(\tau), \tag{15}$$

where $\tau = t' - t$, $\xi(\tau) = -\Omega_\alpha \tau/2 + \tan^{-1}[g(\tau)] - \tan^{-1}[g(0)]$, and $g(\tau) = [(1+\kappa)\tan(\Omega_\alpha \tau/2 + \theta) + s(\kappa)]/\kappa$. Noting the following relation:

$$\frac{\partial\phi}{\partial r'}\frac{\partial}{\partial v_r'} + \frac{1}{r'}\frac{\partial\phi}{\partial\theta'}\frac{\partial}{\partial v_\theta'} = \left(\frac{\partial\phi}{\partial r'}v_r' + \frac{1}{r'}\frac{\partial\phi}{\partial\theta'}v_\theta'\right)\frac{1}{v_\perp}\frac{\partial}{\partial v_\perp}$$
$$= \left[\frac{d\phi(\mathbf{r}', t')}{dt'} - \frac{\partial\phi}{\partial t'} - v_z\frac{\partial\phi}{\partial z'}\right]\frac{1}{v_\perp}\frac{\partial}{\partial v_\perp}.$$

Equation (4) is rewritten as

$$f_\alpha(r,\theta,z,\mathbf{v},t) = \frac{n_{\alpha 0}e_\alpha}{m_\alpha}\left\{\phi\frac{1}{v_\perp}\frac{\partial F_{\alpha 0}}{\partial v_\perp} - \int_{-\infty}^{t} dt'\left[\left(\frac{\partial\phi}{\partial t'} + v_z\frac{\partial\phi}{\partial z'}\right)\frac{1}{v_\perp}\frac{\partial F_{\alpha 0}}{\partial v_\perp} - \frac{\partial\phi}{\partial z'}\frac{\partial F_{\alpha 0}}{\partial v_z}\right]\right\}. \tag{16}$$

Introducing the Fourier-Hankel transform

$$\phi(r,\theta,z,t) = \sum_{\mathbf{k}}\sum_{\ell}\phi_\ell(k_\perp,k_z,\omega)e^{i\ell\rho}\sum_m J_m(k_\perp r)e^{im(\theta-\rho+\pi/2)}e^{i(k_z z-\omega t)},$$
$$= \sum_{\mathbf{k}}\sum_{\ell}\phi_\ell(k_\perp,k_z,\omega)J_\ell(k_\perp r)e^{i\ell(\theta+\pi/2)}e^{i(k_z z-\omega t)}, \tag{17}$$

where $\mathbf{k}_\perp = (k_\perp\cos\rho, k_\perp\sin\rho)$ and integration over ρ is done, the second term of the right hand side of Eq. (16) is rewritten as

$$i\sum_{\mathbf{k}}\int\frac{d\omega}{2\pi}\left[\frac{\omega - k_z v_z}{v_\perp}\frac{\partial F_{\alpha 0}}{\partial v_\perp} + k_z\frac{\partial F_{\alpha 0}}{\partial v_z}\right]\sum_\ell\phi_\ell(k_\perp,k_z,\omega)J_\ell(k_\perp r)e^{i\ell(\theta+\pi/2)}e^{i(k_z z-\omega t)}$$
$$\times\int_{-\infty}^{0} e^{ik_\perp r'\cos(\theta'-\rho)-i(\omega-k_z v_z)\tau}d\tau. \tag{18}$$

Substituting Eqs. (14) and (15) into the integrand over τ of Eq. (18), we obtain

$$f_{\alpha\ell}(r,k_z,\mathbf{v},\omega) = \frac{n_{\alpha 0}e_\alpha}{m_\alpha}\sum_{k_\perp}\phi_\ell\left\{J_\ell(k_\perp r)e^{i\ell\pi/2}\frac{1}{v_\perp}\frac{\partial F_{\alpha 0}}{\partial v_\perp} + i\left(\frac{\omega - k_z v_z}{v_\perp}\frac{\partial F_{\alpha 0}}{\partial v_\perp} + k_z\frac{\partial F_{\alpha 0}}{\partial v_z}\right)\right.$$
$$\times\sum_m J_m(k_\perp r)\sum_{m_1}\cdots\sum_{m_4}J_{m_1}(\beta)\cdots J_{m_4}(\beta)\delta[\ell - (m + m_1 - m_2 - m_3 + m_4)]$$
$$\left.\times e^{im\pi/2}e^{i(m_1+m_2-m_3-m_4)\varphi}\int_{-\infty}^{0} d\tau e^{-i[\omega-k_z v_z-(m_1+m_2)\Omega_\alpha]\tau - i\ell\xi(\tau)}\right\}, \tag{19}$$

where the δ-function comes from the integration over ρ, and $\beta = k_\perp r_L p(\kappa)J_2(Q(\kappa)) \simeq k_\perp r_L/2$. In the above integration over time, the contribution from $\xi(\tau)$ is effective only when $\ell \neq 0$. However, in the experiment, the potential is maximum at the center. Therefore, we may consider the symmetric case $\ell = 0$ for which $\xi(\tau)$ has no longer contribution in the integration over time and it may be neglected in Eq. (19).

Now, the current is evaluated with Eq. (19) as follows:

$$\mathbf{j}_\ell(r,k_z,\omega) = \sum_\alpha\int e_\alpha\mathbf{v}f_{\alpha\ell}(r,k_z,\mathbf{v},\omega)d\mathbf{v}. \tag{20}$$

The radial, azimuthal, and axial components of the current are derived in Appendix and given by

$$4\pi j_{\ell r}(r,k_z,\omega) = \frac{i}{8}\sum_\alpha\sum_{k_\perp}\sum_{m=-\infty}^{\infty}\phi_\ell(k_\perp,k_z,\omega)\left\{[J_{\ell-1}(k_\perp r) - J_{\ell+1}(k_\perp r)]\int\frac{2mv_\perp}{\beta}J_m^2(\beta)[\Lambda(2m+1)\right.$$
$$\left.+\Lambda(2m-1)]d\mathbf{v} - [J_{\ell-1}(k_\perp r) + J_{\ell+1}(k_\perp r)]\int 2v_\perp J_m(\beta)J_m'(\beta)[\Lambda(2m+1) - \Lambda(2m-1)]d\mathbf{v}\right\}, \tag{21}$$

$$4\pi j_{\ell\theta}(r,k_z,\omega)=\frac{1}{8}\sum_{\alpha}\sum_{k_\perp}\sum_{m=-\infty}^{\infty}\phi_\ell(k_\perp,k_z,\omega)\Big\{[J_{\ell-1}(k_\perp r)+J_{\ell+1}(k_\perp r)]\int\frac{2mv_\perp}{\beta}J_m^2(\beta)[\Lambda(2m+1)+\Lambda(2m-1)]d\mathbf{v}$$
$$-[J_{\ell-1}(k_\perp r)-J_{\ell+1}(k_\perp r)]\int 2v_\perp J_m(\beta)J_m'(\beta)[\Lambda(2m+1)-\Lambda(2m-1)]d\mathbf{v}\Big\}, \tag{22}$$

$$4\pi j_{\ell z}(r,k_z,\omega)=\sum_{\alpha}\sum_{k_\perp}\sum_{m=-\infty}^{\infty}\phi_\ell(k_\perp,k_z,\omega)J_\ell(k_\perp r)\times\int v_z J_m(\beta)^2\Lambda_{2m}(\mathbf{v})d\mathbf{v}, \tag{23}$$

where

$$\Lambda_{(2m+1)}(\mathbf{v})=\frac{\omega_\alpha^2}{\omega-k_z v_z-(2m+1)\Omega_\alpha}\times\left[\frac{(2m+1)\Omega_\alpha}{v_\perp}\frac{\partial F_{\alpha0}}{\partial v_\perp}+k_z\frac{\partial F_{\alpha0}}{\partial v_z}\right]. \tag{24}$$

Note that the odd and even cyclotron resonances appear separately in the direction perpendicular and parallel to the magnetic field, which is in contrast to the case in an unbounded plasma, where the resonances are independent on the direction. This is because in the cylindrical system, the particle orbit is modified by the centrifugal force in the direction perpendicular to the magnetic field. Using the following relations:

$$E_{\ell r}(r,k_z,\omega)=-\sum_{k_\perp}\frac{k_\perp}{2}\phi_\ell(k_\perp,k_z,\omega)[J_{\ell-1}(k_\perp r)-J_{\ell+1}(k_\perp r)], \tag{25}$$

$$E_{\ell\theta}(r,k_z,\omega)=-i\sum_{k_\perp}\frac{k_\perp}{2}\phi_\ell(k_\perp,k_z,\omega)[J_{\ell-1}(k_\perp r)+J_{\ell+1}(k_\perp r)], \tag{26}$$

$$E_{\ell z}(r,k_z,\omega)=-i\sum_{k_\perp}k_z\phi_\ell(k_\perp,k_z,\omega)J_\ell(k_\perp r), \tag{27}$$

the current is expressed by

$$4\pi\mathbf{j}_\ell=\begin{pmatrix}-iK_1/k_\perp & K_2/k_\perp & 0\\ -K_2/k_\perp & -iK_1/k_\perp & 0\\ 0 & 0 & -iK_3/k_z\end{pmatrix}\begin{pmatrix}E_{\ell r}\\ E_{\ell\theta}\\ E_{\ell z}\end{pmatrix}, \tag{28}$$

where

$$K_1=\frac{1}{2}\sum_{\alpha}\sum_{m=-\infty}^{\infty}\int\frac{mv_\perp}{\beta}J_m^2(\beta)[\Lambda_{2m+1}(\mathbf{v})+\Lambda_{2m-1}(\mathbf{v})]d\mathbf{v},$$

$$K_2=\frac{1}{2}\sum_{\alpha}\sum_{m=-\infty}^{\infty}\int v_\perp J_m(\beta)J_m'(\beta)[\Lambda_{2m+1}(\mathbf{v})-\Lambda_{2m-1}(\mathbf{v})]d\mathbf{v},$$

$$K_3=\sum_{\alpha}\sum_{m=-\infty}^{\infty}\int v_z J_m^2(\beta)\Lambda_{2m}(\mathbf{v})d\mathbf{v}.$$

Substituting the current into Eq. (2) gives the electric displacement as

$$\mathbf{D}=\begin{pmatrix}K_\perp & iK_{\perp2} & 0\\ -iK_{\perp2} & K_\perp & 0\\ 0 & 0 & K_z\end{pmatrix}\begin{pmatrix}E_r\\ E_\theta\\ E_z\end{pmatrix}, \tag{29}$$

where $K_\perp=1+K_1/\omega k_\perp$, $K_{\perp2}=K_2/\omega k_\perp$, and $K_z=1+K_3/\omega k_z$. For the Maxwellian $F_{\alpha0}$, we have

$$K_\perp=1+\sum_{\alpha}\frac{1}{k_\perp^2\lambda_\alpha^2}\sum_m d_m(\eta)\frac{2m\Omega_\alpha}{k_z v_T}\frac{W(\zeta_{2m+1})+W(\zeta_{2m-1})}{2}, \tag{30}$$

$$K_{\perp2}=\sum_{\alpha}\frac{\Omega_\alpha}{k_\perp v_{T\alpha}}\frac{\omega_\alpha^2}{\Omega_\alpha^2}\sum_m[I_m'(\eta)-I_m(\eta)]\times\frac{W(\zeta_{2m+1})-W(\zeta_{2m-1})}{2}, \tag{31}$$

$$K_z=1+\sum_{\alpha}\frac{1}{k_z^2\lambda_\alpha^2}\left[1+\sum_m d_m(\eta)\zeta_{2m}W(\zeta_{2m})\right], \tag{32}$$

where $d_m(\eta)=I_m(\eta)e^{-\eta}$, $\eta=k_\perp^2 r_L^2/4$, and $W(\zeta)$ are the plasma dispersion function defined by

$$W(\zeta)=\frac{1}{\sqrt{2\pi}}\int_C\frac{1}{x-\zeta}e^{-x^2/2}dx,\quad \zeta_{2m}=\frac{\omega-2m\Omega_\alpha}{k_z v_{T\alpha}}. \tag{33}$$

In deriving Eqs. (30)–(32), we have used the following relations:

$$\int_0^\infty uJ_n(\alpha u)J_n(\beta u)e^{-u^2}du=\frac{1}{2}I_n\left(\frac{\alpha\beta}{2}\right)e^{-(\alpha^2+\beta^2)/4},$$
$$\sum_n J_n(\eta_\alpha)^2=1,\quad \sum_n I_n(\eta_\alpha)e^{-\eta_\alpha}=1.$$

The dispersion relation is determined by the boundary conditions, and this is presented in Secs. III–V.

III. BOUNDARY CONDITIONS AND DISPERSION EQUATION

Since the plasma is detached from the wall, the boundary conditions are that the normal displacement D_r from Eq. (29) and tangential electric fields E_θ from Eq. (26), are continuous at the plasma boundary. Outside the plasma, the potential is a solution of the Laplace equation

$(\nabla_\perp^2 - k_z^2)\ \phi_{out} = 0$ with the condition $\phi_{out}(k_z R) = 0$ at the wall $r = R$, that is,

$$\phi_{out}(k_z r) = A[K_\ell(k_z R) I_\ell(k_z r) - I_\ell(k_z R) K_\ell(k_z r)],$$

where K_ℓ and I_ℓ are the modified Bessel functions of the order ℓ. Therefore, the boundary conditions are combined to give

$$K_\perp k_\perp \frac{J'_\ell(k_\perp r_*)}{J_\ell(k_\perp r_*)} - \frac{\ell}{r_*} K_{\perp 2} = k_z \frac{K_\ell(k_z R) I'_\ell(k_z r_*) - I_\ell(k_z R) K'_\ell(k_z r_*)}{K_\ell(k_z R) I_\ell(k_z r_*) - I_\ell(k_z R) K_\ell(k_z r_*)}, \quad (34)$$

for which we put $\ell = 0$. In addition to the boundary condition, the wavenumber $k_\perp$ is determined from Eq. (2). Substituting Eq. (28) into Eq. (2), we obtain

$$K_\perp \left\{ \frac{1}{r} \frac{\partial}{\partial r} \left[r \frac{\partial}{\partial r} J_\ell(k_\perp r) \right] - \frac{\ell^2}{r^2} J_\ell(k_\perp r) \right\} - k_z^2 K_z J_\ell(k_\perp r) = 0, \quad (35)$$

from which $k_\perp$ is determined by

$$k_\perp^2 K_\perp + k_z^2 K_z = 0. \quad (36)$$

Thus, the waves are determined by solving Eqs. (34) and (36) for which the plasma is assumed to be $\Omega_+ = \Omega_- = \Omega$, $v_{T+} = v_{T-} = v_T$, $\omega_+^2 = \omega_-^2 = \omega_p^2$, and $\lambda_+^2 = \lambda_-^2 = \lambda^2$. The parameters used here are the same as those in the experiment: the density $n_0 = 1 \times 10^8\,\mathrm{cm}^{-3}$ of the fullerene plasma with $m_i = 720\, m_p$ ($\omega_p/2\pi = 78.2\,\mathrm{KHz}$), the magnetic field $B = 0.2$ T ($\Omega/2\pi = 4.2\,\mathrm{KHz}$), the temperature $T_+ = T_- = 0.3\,\mathrm{eV}$ (in the experiment $T_+ \sim T_- \sim 0.3 - 0.5\,\mathrm{eV}$), the plasma radius $r_* = 1.5\,\mathrm{cm}$, and the vessel radius $R = 4\,\mathrm{cm}$, respectively.

For the plasma satisfying the inequality $\omega_p > \Omega > k_z v_T$, we may rely on the asymptotic expansion of the plasma dispersion function in Eqs. (34) and (36), and we obtain

$$1 - G(k_\perp, k_z) = \frac{2}{k_\perp^2 \lambda^2} \sum_{m=-\infty}^{\infty} d_m C_1(m, x), \quad (37)$$

$$k_\perp^2 = -k_z^2 + \frac{2}{\lambda^2} \sum_{m=-\infty}^{\infty} d_m [C_0(m, x) + C_1(m, x)], \quad (38)$$

where $k^2 = k_\perp^2 + k_z^2$, $x = \omega/\Omega$,

$$C_1(m, x) = \frac{2m(2m+1)}{x^2 - (2m+1)^2} + \frac{6m(2m+1) k_z^2 r_L^2}{[x^2 - (2m+1)^2]^2},$$

$$C_0(m, x) = \frac{k_z^2 r_L^2}{x^2 - (2m)^2} + \frac{2(2m)^2 k_z^2 r_L^2}{[x^2 - (2m)^2]^2},$$

and

$$G(k_\perp, k_z) = \frac{k_z}{k_\perp} \frac{J_0(k_\perp r_*)}{J'_0(k_\perp r_*)} \frac{K_0(k_z R) I'_0(k_z r_*) - I_0(k_z R) K'_0(k_z r_*)}{K_0(k_z R) I_0(k_z r_*) - I_0(k_z R) K_0(k_z r_*)}.$$

Equations (37) and (38) give an alternative dispersion equation

$$\frac{1}{2} [k_z^2 + k_\perp^2 G(k_\perp, k_z)] \lambda^2 = \sum_{m=-\infty}^{\infty} d_m C_0(m, x). \quad (39)$$

In the following, we solve Eq. (37) or (39) to get $\omega = \omega(k_\perp, k_z)$ and substitute the result into Eq. (38) to get the relation between k_z and $k_\perp$ numerically. As is shown in Eqs. (37) and (39), the odd and even cyclotron resonances are separated. The coefficient $d_m(\eta)$ is rapidly decreasing with m and increasing with η, thus the higher order resonances become effective for larger η. The reason we retain up to the second order expansion of the plasma dispersion function is because it plays a definite role in the vicinity of the resonance. In the experiment, the Larmor radius is comparable to the half of the vessel radius, implying the waves of higher m are excitable.

In the cyclotron frequency range including higher harmonics waves are basically confined in each interval of the neighboring ion cyclotron resonances in a way that the zeros of the dispersion equations stay in one interval and may not jump the infinite barrier at the resonance. The zeros of the dispersion equation in each interval appear or disappear depending on the wavenumber under the influence of the remote resonances. When the wavenumber increases, the zeros of the dispersion equation move to the lower or upper bound of the interval. Thus, backward and forward waves are rich in pair-ion plasmas since both positive and negative ions contribute to the dispersion equations with the same weight. This is very different from ordinary plasmas, where electrons and ions do not contribute to the dynamics in the same frequency.

IV. BACKWARD WAVES

In the experiment, two branches of backward waves are reported in the low and intermediate frequency ranges although the low frequency backward wave is clearly observed only when waves are excited by a grid exciter. To the best of our knowledge, so far nobody has tried to explain this low frequency backward branch. Here, we show that all backward branches follow from the same physical picture and can be described following the same classic kinetic theory.

A. Low frequency backward waves

Since the backward wave in the interval $0 < \omega < \Omega$ is supposed to be a coupled mode of the thermal and ion cyclotron modes, we substitute $k_\perp^2$ from Eq. (38) into (37) and keep terms with resonances in this frequency range to obtain

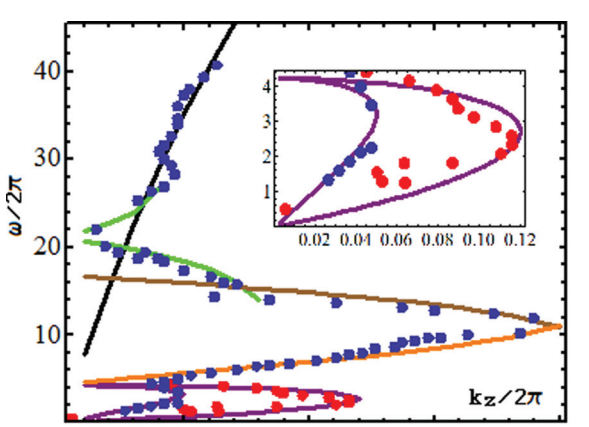

FIG. 1. The dispersion relations of the axially propagating waves of $\ell = 0$. The low frequency backward and forward waves given by Eq. (41) in purple are coupled waves of the ion cyclotron and ion thermal modes for which the enlarged figure of the dispersion relations is embedded. The intermediate frequency backward waves are originated in two different branches, one in brown given by Eq. (43) from the even resonance and the other in green given by Eq. (45) from odd resonance. The intermediate frequency forward wave in orange is the ion cyclotron wave given by Eq. (47) and the high frequency wave in black is the ion Langmuir wave given by Eq. (48). The dots are experimental data with the cylindrical exciter (in blue) and the grid exciter (in red) for references.

$$d_0 \frac{k_z^2 r_L^2}{x^2} - \hat{G} d_1 \left[\frac{2}{x^2-1} + \frac{6k_z^2 r_L^2}{(x^2-1)^2} \right] - \frac{k_z^2 \lambda^2}{2} = 0, \tag{40}$$

where $\hat{G} = G/(1-G)$. For the low frequency oscillation, we may use the plasma approximation and neglect the last term of Eq. (40), which yields

$$\omega^2 = \frac{b_1}{b_2}\Omega^2 \left(1 \pm \sqrt{1 - d_0 k_z^2 r_L^2 b_2 / b_1^2} \right), \tag{41}$$

where $b_1 = d_0 k_z^2 r_L^2 - \hat{G} d_1 (1 - 3k_z^2 r_L^2)$ and $b_2 = d_0 k_z^2 r_L^2 - 2\hat{G} d_1$. This is substituted into Eq. (38) to fix the relation between $k_\perp$ and k_z. The solution Eq. (41) is depicted by the purple curves in Fig. 1: the solutions with + and − signs are backward and forward, respectively. In Fig. 1, the dots are experimental data for references: the blue dots are for the waves excited by a cylindrical exciter and the red ones are by a grid exciter. Since the difference is observed only for the low frequency waves, the experimental data by the grid exciter are plotted only for the low frequency backward and forward waves. The solution (41) fits the data by the cylindrical exciter for the parameters mentioned above. The dispersion curves are terminated at $k_z/2\pi \sim 0.05$, where the solution Eq. (41) becomes complex. The $k_\perp$ is almost constant around $k_\perp r_* \sim 1.035$ and less than the first zero of the eigenfunction $J_0(k_\perp r)$. The data by the grid exciter are reproduced by the same solution (41) with $T = 0.1$ eV and $k_\perp r_* \sim 4.065$, which is between the first and the second zeros of the eigenfunction. For both cases $G(k_\perp, k_z) > 0$, implying the low frequency backward and forward waves do not induce surface charges. As is known from the plasma approximation, the positive and negative ions are in phase. Hence, our theory is able to reproduce and describe, both quantitatively and qualitatively, the excitation by grid and by cylindrical exciter. This is the first successful description of these fine experimentally observed features.

B. Intermediate frequency backward wave

This intermediate frequency mode has grabbed the attention of researchers ever since its discovery.[2] Numerous attempts of explanation of its features in the past decade have failed, and the mode and its properties have remained elusive so far. In the past, this wave is regarded to be from single dispersion curve. However, based on our dispersion Eqs. (37) and (39), the experimental data are supposed to consist of two branches, one from the even resonance Eq. (39) and the other from the odd resonance Eq. (37). First, we consider the frequency range $3\Omega < \omega < 4\Omega$ for which Eq. (39) is written as

$$\frac{1}{2}\left(k_z^2 + k_\perp^2 G\right)\lambda^2 = \sum_{m \neq \pm 2} d_m C_0(m,x) + \frac{64 d_2 k_z^2 r_L^2}{\left(x^2-16\right)^2}. \tag{42}$$

The solution of Eq. (42) is approximated by

$$\frac{\omega^2}{\Omega^2} = 16 - \left[\frac{64 d_2 k_z^2 r_L^2}{(k_z^2 + k_\perp^2 G)\lambda^2/2 - b_3} \right]^{1/2}, \qquad b_3 = \sum_{m \neq \pm 2} d_m C_0(m,4). \tag{43}$$

Equation (43) is substituted into Eq. (37) to get the sets of $k_\perp$ and k_z. The solution Eq. (43) is depicted in Fig. 1 by the brown curve. In the experiment, long wave part of the dispersion relation is not observed, while Eq. (43) does not give a cut-off. It might be due to the rough approximation used above. The $k_\perp r_*$ is around 3.863 between the first and second zeros of the eigenfunction and $G(k_\perp, k_z) > 0$.

In the frequency range $3\Omega < \omega < 5\Omega$, Eq. (37) reads

$$(1-G)\frac{k_\perp^2 \lambda^2}{2} = \sum_{m \neq 3,2} d_m C_1(m,x) + \frac{60 d_2 k_z^2 r_L^2}{\left(x^2-25\right)^2} \tag{44}$$

and the solution is approximately given by

$$\frac{\omega^2}{\Omega^2} = 25 \pm \left[\frac{60 d_2 k_z^2 r_L^2}{(1-G)k_\perp^2 \lambda^2/2 - b_4} \right]^{1/2}, \qquad b_4 = \sum_{m \neq 3,2} d_m C_1(m,5). \tag{45}$$

The solution Eq. (45) with − sign is in the frequency range $3\Omega < \omega < 5\Omega$ and it is depicted in Fig. 1 by the green curve. The dispersion relation of this wave is terminated at the wavenumber at $k_z/2\pi = 0.08$ for the backward wave beyond which $G(k_\perp, k_z) \geq 1$. The $k_\perp r_*$ is around 1.452 for which b_4 is neglected, that is, the effects of the remote resonances are neglected. The similar solution is obtained for large $k_\perp$ for which b_4 is no longer negligible. In this case, $k_\perp r_* \sim 7.275$ and the eigenfunction has two nodes. This is because for the

finite b_4, $G(k_\perp, k_z)$ has to be negative and the real solution of Eq. (45) exists only for large $k_\perp r_*$. The solution Eq. (45) with + sign is a forward wave discussed below.

C. High frequency backward waves

In the frequency range $\omega > 5\Omega$, Eq. (37) does not give real solutions for the ion cyclotron harmonic waves. However, in the experiment, there is a tiny fragment of the dispersion curve of the backward wave at $\omega \sim 7\Omega$. The solution methods have to be contrived.

V. FORWARD WAVES

Three forward waves are observed in the experiment. The low frequency ion thermal wave is already discussed. Here, we discuss the intermediate frequency wave which is the ion cyclotron wave, and the high frequency wave which is the ion Langmuir wave.

A. Ion cyclotron harmonic waves

For the frequency range $\Omega < \omega < 3\Omega$, we solve Eq. (37)

$$(1-G)\frac{k_\perp^2\lambda^2}{2} = \sum_{m\neq -1} d_m C_1(m,x) + \frac{6d_1 k_z^2 r_L^2}{(x^2-1)^2}, \tag{46}$$

where the term $2d_1/(x^2-1)$ is neglected since this term is dominated over by the second term of the right hand side. The solution is given by

$$\frac{\omega^2}{\Omega^2} = 1 + \left[\frac{6d_1 k_z^2 r_L^2}{(1-G)k_\perp^2\lambda^2/2 - b_5}\right]^{1/2}, \qquad b_5 = \sum_{m\neq -1} d_m C_1(m,1). \tag{47}$$

The solution is depicted in Fig. 1 by the orange curve. The $k_\perp r_*$ is around 0.39 and $G(k_\perp, k_z) > 0$.

Above the frequency range $\omega \sim 5\Omega$, the observed fragment of the dispersion curve of the forward wave is given by the solution Eq. (45) with + sign and is shown in green in Fig. 1. The branch is terminated at $k_z/2\pi = 0.04$ and $k_\perp r_* \sim 1.313$.

B. Ion Langmuir wave

In the high frequency range $\omega \gg \Omega$, Eq. (37) gives $G(k_\perp, k_z) = 1$ which determines the relation between $k_\perp$ and k_z. Here, $k_\perp$ is almost proportional to k_z ($k_\perp$ changes from 0.845 to 1.117 when $k_z/2\pi$ changes from 0.01 to 0.20) and certainly $k_\perp r_*$ is less than the first zero of the eigenfunction. Then, we solve Eq. (39) in which we keep only the term of $m = 0$ to give

$$\omega^2 = \frac{2d_0 k_z^2}{k_\perp^2 + k_z^2}\omega_p^2. \tag{48}$$

This is the ion Langmuir wave in a cylindrical system and it is depicted in Fig. 1 by a black curve. Note that in Ref. 4, the density estimated from the dispersion relation $\omega = \sqrt{2}\omega_p$ is 3.3×10^6 although the value measured by the probe is 10^8. This discrepancy is resolved by using our derived expression, which fits the experimental data with $n = 10^8$.

VI. DISCUSSION

In summary, we have studied the propagation characteristics of electrostatic waves in homogeneous bounded pair-ion plasma in a cylindrical system. We have shown analytically based on a kinetic theory that the experimentally observed[1–5] backward waves are ion cyclotron harmonic waves in the intermediate frequency range, and a coupled wave of ion cyclotron mode and ion thermal mode in the low frequency range. In pair-ion plasmas, positive and negative ions respond to potential in the same time scale, and their orbital property reflects in wave propagation characteristics. In addition, the large Larmor radius is crucial for higher harmonic cyclotron resonances to play definite roles in the dispersion equations and makes the first few harmonic ion cyclotron waves observable. Thus, a kinetic theory is needed to explain not only backward waves but also fine structure of dispersion relations in pair-ion plasmas.

A most important message of this work could be summarized as follows. The pair-ion fullerene plasma obtained in the laboratory[1–5] is truly a new and exciting research field, which opens up possibility of applications of this knowledge to various other fields like dusty plasma, and in particular, to extremely cold antimatter plasma (consisting of electrons and positrons). Namely, the pair-ion plasma is free of the problem of annihilation inherent in the antimatter plasma, which makes the latter not so suitable for experimental studies. Thus, the knowledge and pair-properties of pair-ion plasma are clearly directly applicable to and can be used in the theory of the antimatter plasma as well. However, in spite of being such an essentially new field, in this work we have shown that the physics of the pair-ion plasma fits perfectly well into the classic kinetic plasma theory.[18] The experimentally observed backward modes consequently come not as a surprise. They are expected and logical part of the classic ion-cyclotron wave behavior in the bounded plasma environment, where kinetic effects play an essential part. The intermediate frequency backward wave has been in the focus of researchers and subject of numerous works in the past decade, and yet it has remained unexplained so far. At the same time, the other backward modes (the low-frequency one has been clearly experimentally verified) have remained unexplored and unexplained. In the present work, we have shown that these two, together with other backward modes that yet remain to be experimentally verified, represent a part of the same global kinetic theory picture.

ACKNOWLEDGMENTS

One of the authors (M.K.) would like to thank Professor H. Saleem for fruitful discussions.

APPENDIX: DERIVATIONS OF EQS. (21)–(23)

The radial component of the current Eq. (21) is obtained as follows:

$$\begin{aligned}4\pi j_{\ell r}(r,k_z,\omega) &= \sum_\alpha e_\alpha \int v_\perp \cos\varphi f_{\alpha\ell}(r,k_z,\mathbf{v},\omega)d\mathbf{v},\\ &= i\sum_\alpha \omega_\alpha^2 \sum_{k_\perp} \phi_\ell(k_\perp,k_z,\omega)\sum_m J_m(k_\perp r)e^{i(m-\ell)\pi/2}\sum_{m_1}\sum_{m_2}\sum_{m_3}\sum_{m_4}\\ &\quad\times \delta[\ell-(m+m_1-m_2-m_3+m_4)]\int v_\perp\left(\frac{\omega-k_z v_z}{v_\perp}\frac{\partial F_{\alpha 0}}{\partial v_\perp}+k_z\frac{\partial F_{\alpha 0}}{\partial v_z}\right)\\ &\quad\times \frac{J_{m_1}(\beta)J_{m_2}(\beta)J_{m_3}(\beta)J_{m_4}(\beta)}{\omega-k_z v_z-(m_1+m_2)\Omega}\cos\varphi e^{i(m_1+m_2-m_3-m_4)\varphi}v_\perp dv_\perp dv_z d\varphi.\end{aligned}$$

The integration over φ gives $\delta(m_1+m_2-m_3-m_4\pm 1)$. Two δ-functions together with the relation $\sum_n J_n(z)J_{n-m}(z)=\delta(m)$, we have $m=\ell\pm 1$ and $m_2=m_1\pm 1$. Eq. (21) is obtained by using the following relations:

$$J_{\ell-1}J_mJ_{m+1}-J_{\ell+1}J_{m-1}J_m=\frac{1}{2}[(J_{\ell-1}-J_{\ell+1})J_m(J_{m-1}+J_{m+1})-(J_{\ell-1}+J_{\ell+1})J_m(J_{m-1}-J_{m+1})],$$

and

$$J_{\ell-1}J_{m-1}J_m-J_{\ell+1}J_mJ_{m+1}=\frac{1}{2}[(J_{\ell-1}-J_{\ell+1})J_m(J_{m-1}+J_{m+1})+(J_{\ell-1}+J_{\ell+1})J_m(J_{m-1}-J_{m+1})].$$

The azimuthal component of the current is obtained in a similar way. The axial component of the current is straightforwardly obtained since v_z is independent of φ and we have $m=\ell$ and $m_2=m_1$.

[1]W. Oohara and R. Hatakeyama, Phys. Rev. Lett. **91**, 205005 (2003).
[2]W. Oohara, D. Date, and R. Hatakeyama, Phys. Rev. Lett. **95**, 175003 (2005).
[3]W. Oohara and R. Hatakeyama, Phys. Plasmas **14**, 055704 (2007).
[4]W. Oohara, Y. Kuwabara, and R. Hatakeyama, Phys. Rev. E **75**, 056403 (2007).
[5]W. Oohara, T. Hibino, T. Higuchi, and T. Ohta, Rev. Sci. Instrum. **83**, 083509 (2012).
[6]J. Vranjes and S. Poedts, Plasma Sources Sci. Technol. **14**, 485 (2005).
[7]H. Schamel and A. Luque, New J. Phys. **7**, 69 (2005).
[8]F. Verheest, Phys. Plasmas **12**, 032304 (2005).
[9]H. Saleem, J. Vranjes, and S. Poedts, Phys. Lett. A **350**, 375 (2006).
[10]F. Verheest, Phys. Plasmas **13**, 082301 (2006).
[11]B. Zhao and J. Zheng, Phys. Plasmas **14**, 062106 (2007).
[12]J. Vranjes, D. Petrovic, B. P. Pandey, and S. Poedts, Phys. Plasmas **15**, 072104 (2008).
[13]J. Vranjes and S. Poedts, Phys. Plasmas **15**, 044501 (2008).
[14]H. Schamel, Phys. Plasmas **16**, 113709 (2009).
[15]F. Anderegg, C. F. Driscoll, D. H. Dubin, T. M. O'Neil, and F. Valentini, Phys. Plasmas **16**, 055705 (2009).
[16]H. Saleem, N. Batool, and S. Poedts, Phys. Plasmas **18**, 052108 (2011).
[17]F. Verheest, Phys. Plasmas **19**, 092302 (2012).
[18]A. W. Trivelpiece and R. W. Gould, J. Appl. Phys. **30**, 1784 (1959).